



# The Superconducting Gravimeter CD-034 at Moxa Observatory: More than 20 Years of Scientific Experience and a Reanimation

T. JAHR<sup>1</sup> and R. STOLZ<sup>2</sup>

**Abstract**—In this work, advanced methods and processing schemes for the analysis of data from a Superconducting Gravimeter (SG) will be introduced and their relevance on acquired data proved. The SG CD-034 was installed on Easter of 1999 in the Geodynamic Observatory Moxa of the Friedrich Schiller University Jena, Germany. Initially, the quality of the recorded data was examined, spectra for the detection of the parasitic modes were calculated and the calibration values for the two sensors were determined. Ever since very high-quality gravity data of this SG and most of the other worldwide SGs were made available through the storage archive of the Global Geodynamics Project (GGP later changed to IGETS, International Geodynamics and Earth Tide Service) for global scientific investigations at that time. SG's such as the one in Moxa (Germany) still deliver significant scientific value for global gravitational field studies as well as for regional/local studies which will be shortly reviewed. Examples are the detection of polar motion, the influence of continental water loading in general and in particular river basin loads, the gravimetric effect of North Sea storm surges and the study of hydro-gravimetric signals, which could be compared with satellite observations and global hydraulic models. The long-term, low-noise operation of complex SG's requires some effort on maintenance. In order to evaluate the correct operation of the SG, new data processing steps were introduced to assist in the analysis of the data in case of issues with the instrumentation. For example, in 2012/2013 and 2020/2021 severe interference in the gravimeter electronics in Moxa led to a significant loss of data. In both cases, however, the cause could be determined, and the corresponding electronic components renewed. Since July 2021, the SG in Moxa registers again with high data quality comparable or slightly better than before the incident. Initial tests and tidal analyses confirm the validity of the old calibration factors, and the authors now look forward to the re-established long-term recording with excitement and confidence.

**Keywords:** Superconducting gravimeter, gravity observation, long-term time series, environmental parameters, SG-electronics, tidal analysis.

## 1. Introduction

Today, the monitoring of the evolution of the Earth system is one of the key tasks in the geosciences. The measurement of gravity at utmost accuracy leads to significant impact in mineral exploration, risk assessment and mitigation, subsidence of low-lying areas, ice mass changes, earthquakes, and the investigation of ground water resources, especially by using long duration time series recording of ground-based instruments, see van Camp et al. (2017) and references therein.

Tremendous progress has been made in the past decades of gravimeter instrumentation. There are two main classes, namely absolute and relative gravimeters measuring the absolute gravity value or relative changes of it. Reviews on sensors and instrumentation provide e.g. Niebauer (2015) or van Camp et al. (2017). The focus of this work lays in the application of superconducting gravimeters (SGs) which are up to now the most precise relative gravimeters for terrestrial observation. They are discussed in detail in Hinderer et al., (2007, 2015).

One SG was added, along with advanced tilt and strain measuring instruments, to the existing instrumentation of the Geodynamic Observatory (Fig. 1) in Moxa (Germany) as part of the expansion of the original seismological station at the end of the 1990s (Jahr et al., 2001). The superconducting gravimeter SG CD-034 was installed in April 1999 in the so-called large registration room of the observatory, cf.

<sup>1</sup> Institute of Geosciences, Department of General Geophysics, Friedrich Schiller University Jena (FSU), Burgweg 11, 07749 Jena, Germany. E-mail: thomas.jahr@uni-jena.de

<sup>2</sup> Department of Quantum Systems, Leibniz Institute of Photonic Technology (Leibniz IPHT), Albert-Einstein-Straße 9, 07745 Jena, Germany.

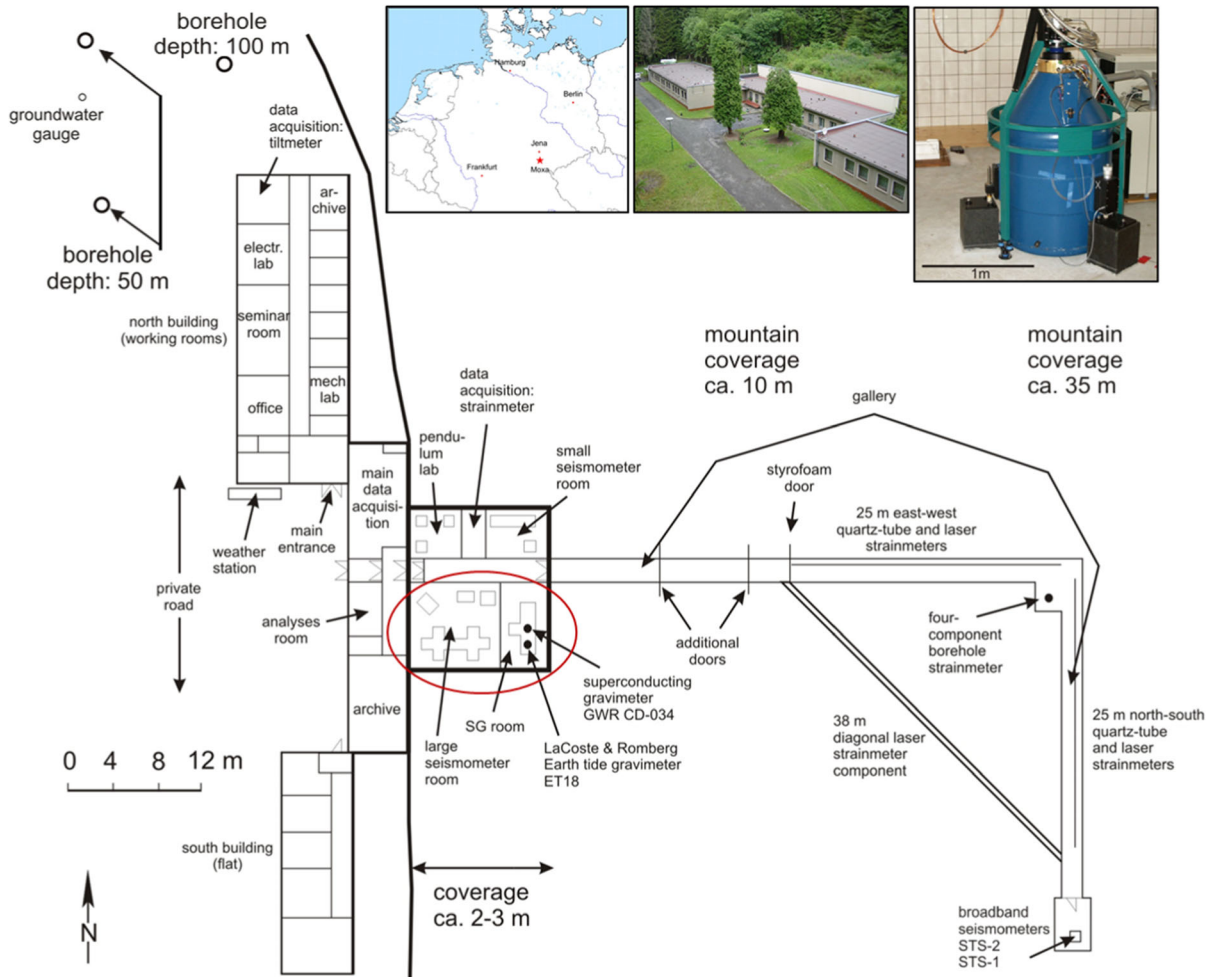


Figure 1

Ground view of the Geodynamic Observatory Moxa. Upper row: location in Germany (left), bird view of Moxa observatory (middle), SG CD-034 installed on a concrete base (right), this location is also marked by the red circle; after Jahr and Weise (2020)

(red circle in Fig. 1), and subsequently brought into continuous operation. The gravimeter instrument itself consist of a dewar with a dual-sphere-sensor system with high long-term stability (Kroner, 2002), a liquid helium refrigeration unit, a dual tilt compensation system and finally a rack with a data acquisition and power supply unit. The whole dewar and tilt compensation system is mounted on a separate foundation than the observatory and the room is temperature stabilized to  $\pm 1$  °C. All environmental conditions inside and around the gravimeter such as temperatures, pressures, wind, precipitation, and tilt are continuously monitored.

The first step after the installation process was primarily to evaluate the data quality and to determine the calibration factors for both sensors. The very good data quality for the seismic sensors in a frequency range of 10mHz up to 100Hz was already reported and discussed by Klinge (2000) and Teupser (1975). For the long gravimetric periods observed by the SG, the observatory in Moxa could be determined by Rosat (2002) as the station with the lowest noise level. As a consequence, the earlier shown low station microseism for the seismological observations apparently also applies to the long periods (tides and longer) of the SG registration. The recent comparison

of the installed SGs is given by Rosat and Hinderer (2011). In addition to the calibration factors, gravimeter-typical variables, such as the frequencies of the parasitic modes (discussed in Sect. 4.1, refer to Fig. 2) representing a horizontal transverse oscillation of the superconducting spheres in the magnetic field, were determined (Kroner, 2002). These frequencies were detected at 27mHz for the lower sensor and 23mHz for the upper sensor (Fig. 3). The stability and analytic properties of those frequencies will be discussed within this work.

For the important determination of the calibration factors, parallel registrations were made both with the Earth tide gravimeter LCR ET-18 and with absolute gravimeters from the BKG (*Bundesamt für Kartographie und Geodäsie*, formerly Frankfurt, now Leipzig), from our Finish colleagues and from Olivier Francis (observatory Walferdange). The LCR ET-18 Gravimeter can be calibrated even on calibration lines. For example, on the points in the Harz mountains or on the vertical calibration line in the high-rise building in Hannover. The parallel registration with the SG in the Observatory Moxa then enables the control of SG calibration factors via the tidal

analyses. The absolute measurements are meanwhile taken twice a year in Moxa Observatory in an adjacent parallel registration procedure. The gained results are used to calibrate both sensors and additionally to control the drift of the SG data. This procedure proved the SG to operate at very low noise levels with minimum deviations.

The article is structured as follows: this first section gives a short introduction on the SG installed in Moxa, its calibration and data quality. The second section addresses the topic, why it is still important to continuously operate and maintain SGs in observatories. The chapter shows examples of latest measurements and scientific results achieved with the SG in the observatory in Moxa. The third section introduces the advanced methods to process the data of the SG which will be used in the subsequent chapters to analyze the data quality. They help to understand the pitfalls of the instrumentation and to reveal new insights. The fourth chapter of this work will cope with the issues related to the gravimeter instrumentation in Moxa itself which led to interrupts in the times series of the SG in 2012/2013 and 2020/2021 and required significant corrections to

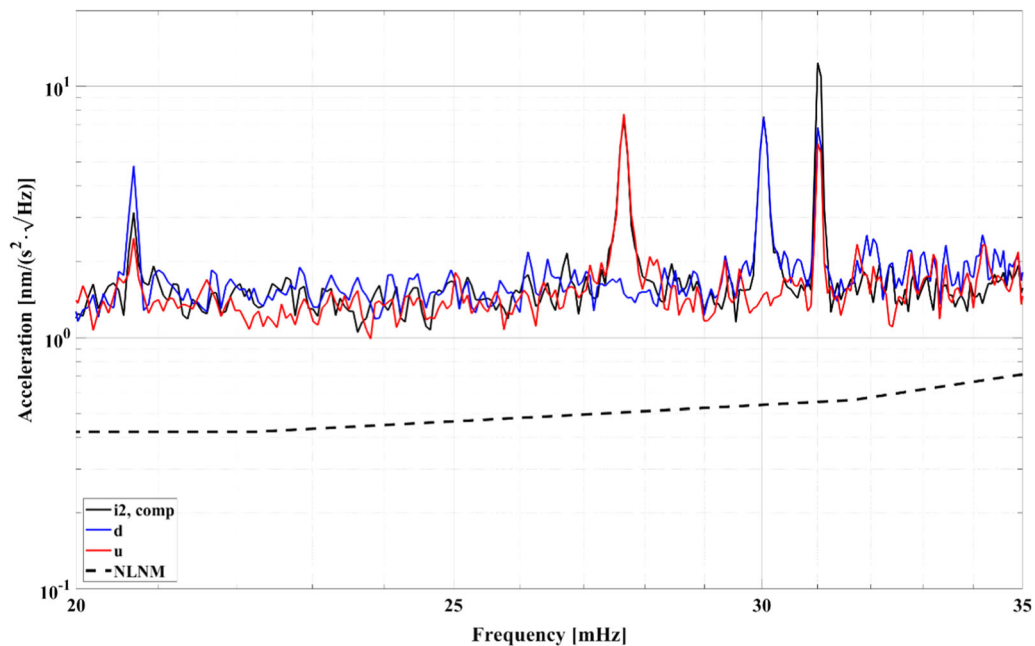


Figure 2  
Zoom into graph in Fig. 3

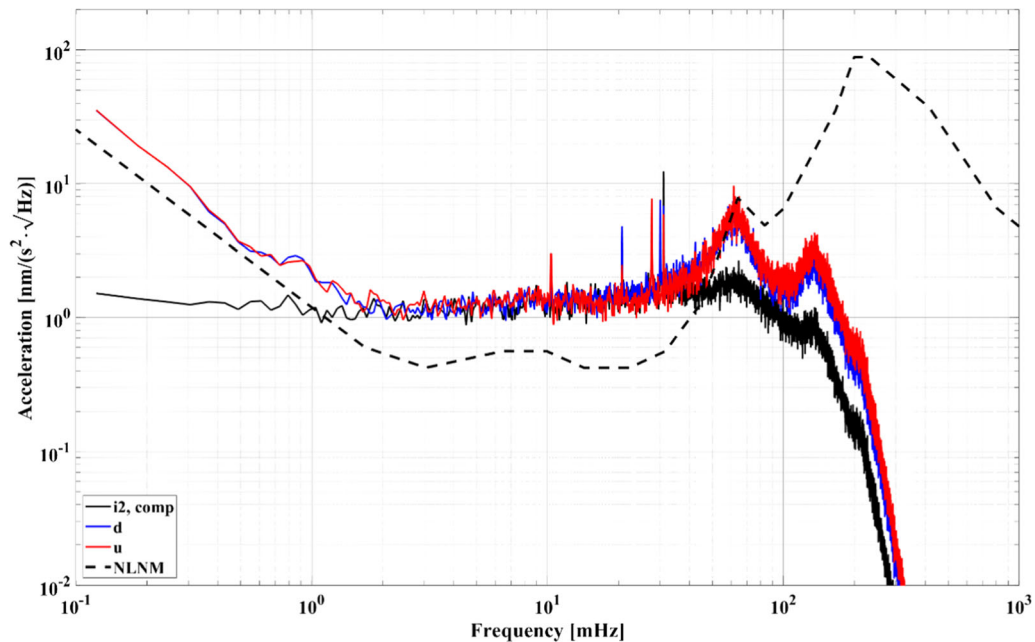


Figure 3

Signals of upper and lower sphere as well as their difference signal (abbreviated as “comp”) shown by the red, blue, and black curve, respectively

bring it into operation again. This section is also informative to other customers of this type of SGs in terrestrial observatories. The fifth section shows latest results of tidal analyses and discusses them in this context. Finally, in the sixth section the results are summarized, and a short outlook is given.

## 2. Scientific Studies with the SG in the Observatory Moxa, Germany

The aim of this section is to motivate the future operation and maintenance of the SGs. Thus, a short review on the successful studies with the SG in the observatory Moxa will be provided hereafter. Although these investigations relate to the specific situation of the Observatory Moxa, they can also be used in the broadest sense in other SG stations. Hydrologically oriented studies, together with the mass movements associated therewith, form an ideal field for the interpretation of long time series which

have been observed with superconducting gravimeters.

### 2.1. Effect of Polar Motion

SG's have been developed to detect tiny gravity changes with very long periods that have a sufficient signal to noise ratio. The pole movement describes the movement of the axis of rotation around the axis of the figure of the earth and thus leads to a small gravity change of  $3 - 8 \mu\text{Gal}$  ( $30 - 80 \text{nm/s}^2$ ) with a period of over one year (Chandler Wobble with about 430 days period as well as the annual wave). For Moxa observatory the gravity effect of polar motion was clearly observed by the SG and reported by Kroner (2002).

### 2.2. Hydrological Induced Gravity Changes

A typical effect for SG recordings at Moxa observatory is given by the local hydrological situation. Usually, the gravity observed by the SG

increases as soon as rain begins because more mass is in the sub-surface space. In Moxa, however, a reduction in gravity was recorded during the rain, which means that the mass increase must have taken place above the SG. This hypothesis could be confirmed by means of a sprinkling test in which 20 tons of extinguishing water were injected from the cistern onto the roof (Kroner & Jahr, 2006; Kroner et al., 2007).

In cooperation with various institutions, in particular the Institute of Geography of the FSU and also the University of Wageningen/Netherlands, a

conceptual *hydrological model* for the observatory environment was developed in the 2000's and made accessible for gravimetry (Krause et al., 2009; Naujoks et al., 2008). Using this very effective correction method, the residuals of the SG in Moxa, c.f. Figure 4, were brought into accordance with satellite-based gravity observations. The procedure, which also requires a transfer of the hydrological model into a time-dependent gravimetric model, can also be understood as methodically exemplary for other SG stations worldwide (Weise & Jahr, 2018; Weise et al., 2009, 2012).

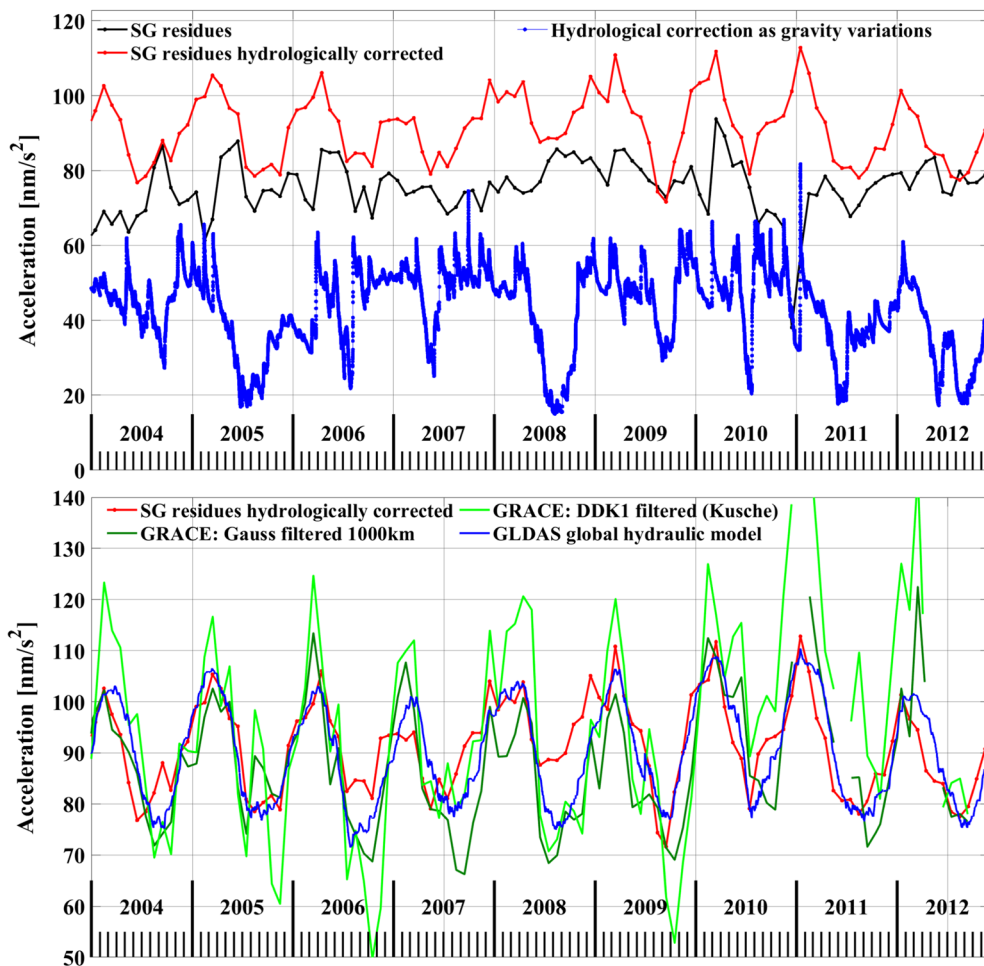


Figure 4

Top panel: Comparison of hydrological correction as gravity variations (blue curve), the original SG residuals from 2004 to 2012 as well as local hydrologically corrected as black and red curves, respectively. Bottom panel: The GLDAS global hydraulic model (blue curve), the differently filtered GRACE data as green curves, and the red curve from the top panel illustrating the correlation observable both in the amplitudes and with respect to the phase position (Weise & Jahr, 2018)



### 2.3. *Effect of Loading From Large River Basins*

In the context of the activities around the Moxa observatory, a study was carried out to investigate the load effect of changing water levels in the large rivers of Central Europe (Kroner & Weise, 2011). For the digitized flow patterns and the respectively prevailing maximum variations of the water levels, the associated gravimetric load effects for Moxa and five further SG stations in Central Europe were calculated (Kroner & Weise, 2011). The result of the load calculations is largely in line with expectations: for Moxa, the Elbe has the most significant influence, while for the SG station Medicina (more than  $3\text{nm/s}^2$ ), the Po dominates, for Strasbourg it is the upper Rhine (more than  $2\text{nm/s}^2$ ). For Moxa, this load of more than  $9\text{nm/s}^2$  is significantly above the achieved resolution of the SG measurements and thus represents a significant contribution to the indirect effect. This result shows that in addition to the ocean tidal loading, the water level changes of big rivers also yield a contribution to the indirect effect in the tidal parameters provided by the tidal analysis.

### 2.4. *Are Storm Surges on the German North Sea Coast Detectable by the SG in the Observatory Moxa?*

On the occasion of the 2013 climate anniversary colloquium in Jena (Goethe's further heritage: 200 years of climate recording station in Jena), the question was raised whether storm surge events on the German North Sea coast, in particular also in the German Bay, via the associated gravimetric charging effect, can be detected or not by our SG in the Observatory Moxa. The resulting study for a storm event at the beginning of 2012 required extensive new data processing of both SG data from Moxa and level data from the observation station at Cuxhaven.

The study shows that a wind driven ocean load signal can be measured, but at the same time strong air pressure fluctuations also occur at the SG location, which are superimposed on this signal. In order to be able to unambiguously detect a storm surge, the three-dimensionally modeled air pressure correction (ATMACS, Klügel & Wziontek, 2009) still needs to

be significantly improved, so that extreme pressure conditions and their gradients and the resulting contributions in the gravity measurements can also be compensated for (Jahr & Weise, 2020).

### 3. *Data Processing and Analyzing Tools for the SG Data*

The common base of all earlier studies in this work is a tidal analysis (e.g. by means of ETERNA3.4, Wenzel, 1996). It enables the elimination of theoretical tides applicable to the station in each case by application of the calculated tidal parameters. The remaining data are referred to as residuals. Often, the barometric air pressure influence is also corrected for as part of this process. As an example, the important residuals for the SG in the Observatory Moxa are shown in Fig. 5 for the period from 2002 to April 2022 inclusive. They were calculated from data of the lower sensor. In addition to the tides of the solid earth, the air pressure effect and the pole movement were eliminated, whereby the theoretical tides were calculated with the observed tidal parameters for Moxa and the air pressure variations were recorded directly next to the SG in a second cycle. The residuals vary by about  $170\text{nm/s}^2$  over the 20 years with a longer gap of 3.5 months at the beginning of 2012. This is due to the first repair interval and shows that the variation of residuals after repair is visibly smaller than before. Both Fig. 4 and Fig. 5 show residues for the lower sensor of the superconducting gravimeter SG-CD034 in the Observatory Moxa. In addition to the different time periods, however, in Fig. 5 hourly values and in Fig. 4 monthly values have been used, because for the correlations shown in Fig. 4, the satellite data are only available in monthly data samples. Nevertheless, both figures contain the same residual information for the corresponding longer, seasonal periods. In addition, a trend towards lower values, i.e. a decrease in gravity, can be detected in 2003/2004, 2007, 2009/2010, 2016 and 2018/2019. This could also be associated with the increasing dryness in the observatory environment, but the effect still needs to be verified by comparing it with absolute gravity values. With these residuals, the local

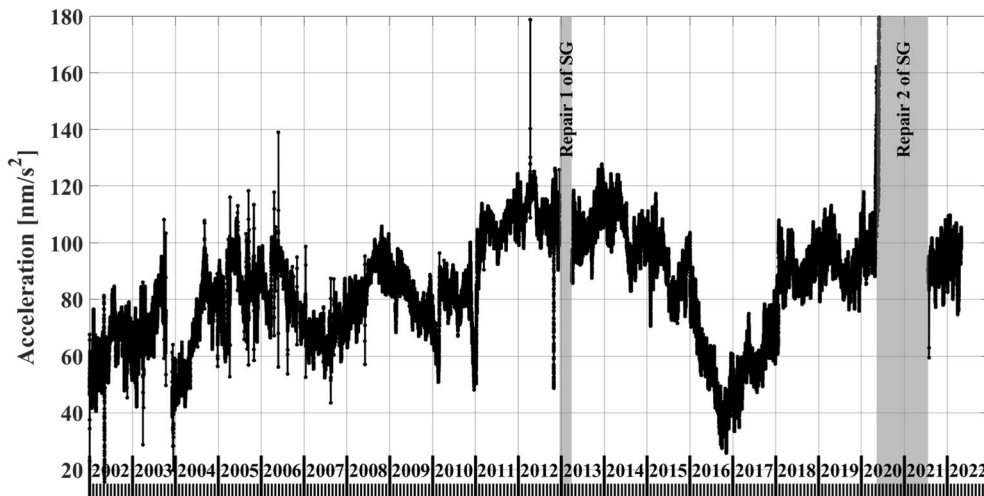


Figure 5

Residuals of 20 years of SG recording at Moxa observatory. The hourly values are observed by the lower sensor and the earth tides, polar motion and barometric pressure effect are subtracted

hydrological/gravimetric investigations, already described herein, can thus be continued in the future.

Although the residuals provide some details of the correct operation of the SG, they still may fail which will be shown in the next section of this work. Kroner (2002) used the average energy–density spectra of the residuals in Fourier space in order to analyze them for their parasitic modes. The example for the SG CD-034 shown therein were calculated from the raw data of five quiet consecutive days. The parasitic modes were found at 27mHz (lower sensor) and at 23mHz (upper sensor). The cause of the other signals at 11mHz and between 25 and 26mHz is unknown. In addition, the noise level of the NLNM (Peterson, 1993) were shown for comparison. However, in this work the analysis of the SG’s data was significantly extended in order to provide a quick and detailed insight whether the SG shows correct and low-noise operation. The SG CD-034 has a specific construction with two superconducting spheres with an approximate vertical distance of 20cm (Richter & Warburton, 1998). The signals of the upper and lower sphere are called  $g_u$  and  $g_d$ , respectively. These factors derived by parallel absolute gravity observations, carried out twice per year by the colleagues from BKG (Bundesamt für Kartographie und Geodäsie, Frankfurt and Leipzig). The official values are:  $-0.606500\text{nm}/(\text{s}^2 \cdot \text{mV})$  for lower sensor  $g_d$ , and

$-0.640098\text{nm}/(\text{s}^2 \cdot \text{mV})$  for upper sensor  $g_u$ . As first step in the processing, these factors are applied for the calibration of the sensor signals.

The next step of the new analysis is to subtract the model of the signal from the tidal analysis, called  $g_t$ , in a least-squares sense using the MATLAB<sup>TM</sup> function *mldivide* using a constant coefficient  $\alpha_u$  and  $\alpha_d$ . For an over-determined system of equations, which is applicable, this function estimates the Moore–Penrose pseudoinverse (Stoer & Bulirsch, 2002). The according residuals are  $r_u = g_u - \alpha_u \cdot g_t$  and  $r_d = g_d - \alpha_d \cdot g_t$ . The coefficients  $\alpha_u$  and  $\alpha_d$  are expected to be almost one. If this is not the case, an issue with the data could be suspected. The new analysis does not, like Kroner (2002), precondition the residuals by using a high-order polynomial. Instead, we make use of the specific construction with the two spheres at a vertical distance. For all sources which are farther away than the distance (= baseline) between the two spheres, the signals should have high correlation coefficients. Thus, by assuming all sources to be far away, which is in most cases valid, one can calculate a difference signal  $\Delta r = r_u - r_d$  which is a response of a first order gravity gradiometer. However, one has to consider that the lower sphere is in a point of lowest tilt sensitivity which will result in a lower noise floor. Most probably there will be also differences in the frequency dependent transfer

function of the two spheres, which will cause only secondary disturbances and hence be neglected for this work.

The final step is to use the residuum  $\Delta r$  for undertaking a joint time–frequency analysis (JTFA) using Matlab<sup>TM</sup>'s *spectrogram* function (Oppenheim & Schaffer, 2014). For the Fourier transformation, Welch's method is used (function *pwelch*, Stoica & Moses, 2005). Both, the Fourier transformation and the JTFA, using a window (block) size of  $2^{14}$  samples with 50% overlap, and a Hanning window. Typically, a time series for one month in the summer is processed and some intervals, called  $ik (k \in \mathbb{N})$  in the figures, of this time series were chosen as well. The intervals were selected using a small standard deviation (in this work abbreviated as 'std') as measure.

#### 4. Analysis of the SG's Operation in the Observatory in Moxa

In this section various time series from 2002 until 2021 were processed and analyzed using the methods described in the previous part of this work.

##### 4.1. Data Quality of the SG After Installation

As a representative example, the July 2002 period has been chosen in order to study very low noise data three years after the installation (Fig. 6). The Fourier spectra of the full time series as well as of some low noise intervals are depicted inside the Fig. 6. There is a white noise floor of about  $1.2 \text{ nm}/(\text{s}^2 \cdot \sqrt{\text{Hz}})$  and down to almost 0.1mHz no low frequency noise onset is observable. The curves for the NLNM and the spectra have a cross-over frequency of about 1mHz. The signal band is 3dB limited to  $\sim 130 \text{ mHz}$ . External signals are observable as rise in the spectral values in the frequency band between about 10mHz to the signal band limit. There is a number of characteristic frequencies observable. Figure 3 depicts the data for interval  $i2$  with the lowest value of the standard deviation. Therein, the residuals  $r_u$  and  $r_d$  as well as the difference signal are shown. The residuals there are slightly higher than the NLNM below the cross-over frequency.

A number of discrete frequency peaks are also visible in Fig. 2 which shows common frequencies such as 20.7mHz and 31.0mHz and separate

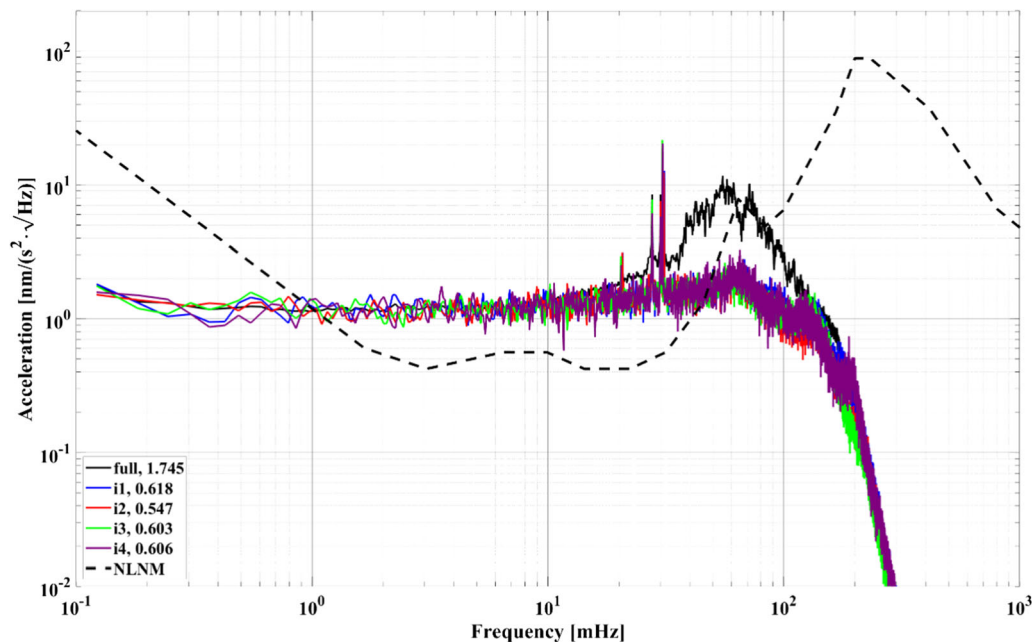


Figure 6

Difference signal  $\Delta r$  of the SG CD-034 for July 2002. The full time series and intervals of it are marked by full and  $ik$  in the legend. The numbers correspond to the according standard deviation in  $\text{nm}_{\text{RMS}}/\text{s}^2$  (RMS – root mean square). The unit of all spectra throughout this work are also in RMS values



frequencies such as 27.6mHz and 30.0mHz in the upper and lower sensor signal, respectively. For the peak at 20.7mHz the lower sensor has the highest amplitude. Since the difference signal is smaller in amplitude the signal of the upper and lower sphere should have a difference in phase. For the 31.0mHz both signals are at the same amplitude and in phase and the residuals are of higher amplitude. The behavior of the peaks at 27.6mHz and 30.0mHz does not agree with Kroner (2002) with frequencies detected at about 27mHz and 23mHz for the lower and upper sensor. The two sensors show at their own specific frequency almost the same signal strength.

In order to understand the evolution of the residuals of the SG, the difference of the signals of the lower and upper sphere, the JTFA is calculated for the July 2002 data set. The results are given in Figs. 7 and 8. Above  $\sim 130$ mHz the noise drops off quite quickly which suggests that this is the limit of the signal band. A number of seismic events are clearly visible as vertical lines. Typically, they excite the band of  $\sim 20$ mHz to  $\sim 100$ mHz. Strong signals as for day 21 can also excite a larger range of frequencies. In Fig. 8 the range of characteristic

frequencies is highlighted. Clearly, the earlier discussed frequencies are observable as horizontal lines. What was not derivable from the pure Fourier spectrum are the behavior of those frequencies. The specific frequencies of the spheres at 27.6mHz and 30.0mHz seem not to change over time. The two other frequencies are changing over time. The variations happen gradually on longer time scales. They show the same behavior but at a different frequency range. The cause of these frequencies is not understood yet. Further detailed investigations are required, in order to determine their course. It could be external conditions such as barometric pressure changes or precipitation. They could also be instrument intrinsic effects such as helium level or compressor operation etc.

#### 4.2. Data and Instrument Issues in 2012/2013 and 2020/2021

In the course of 2012, the data quality of the two sensors of the SG in Moxa gradually changed, with this initially only affecting the upper sensor and the latter only in short intervals. The initial

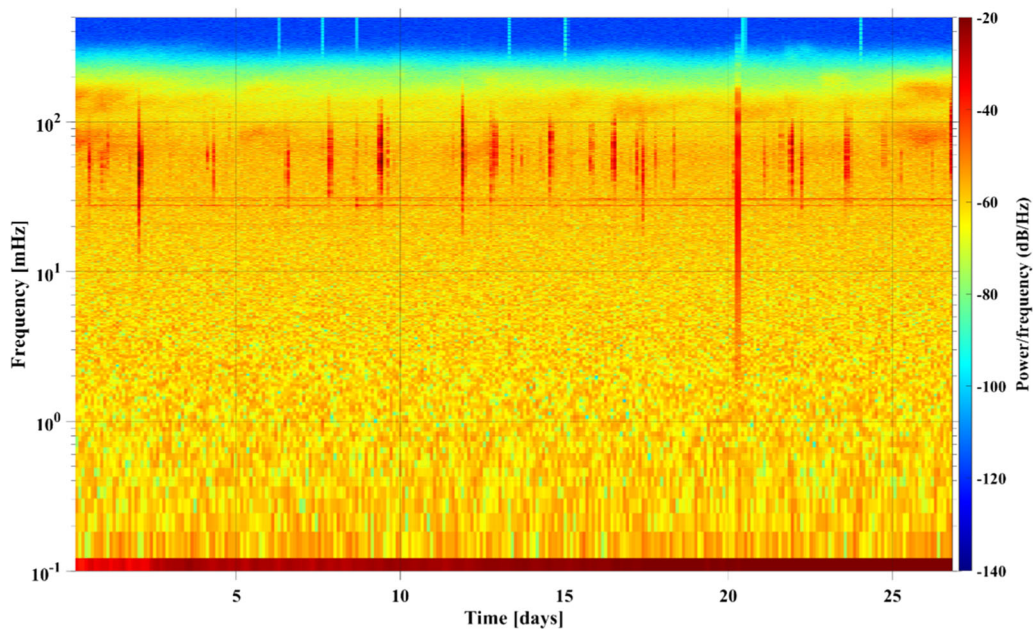


Figure 7  
Residual of the SG recording at Moxa Observatory for July 2002

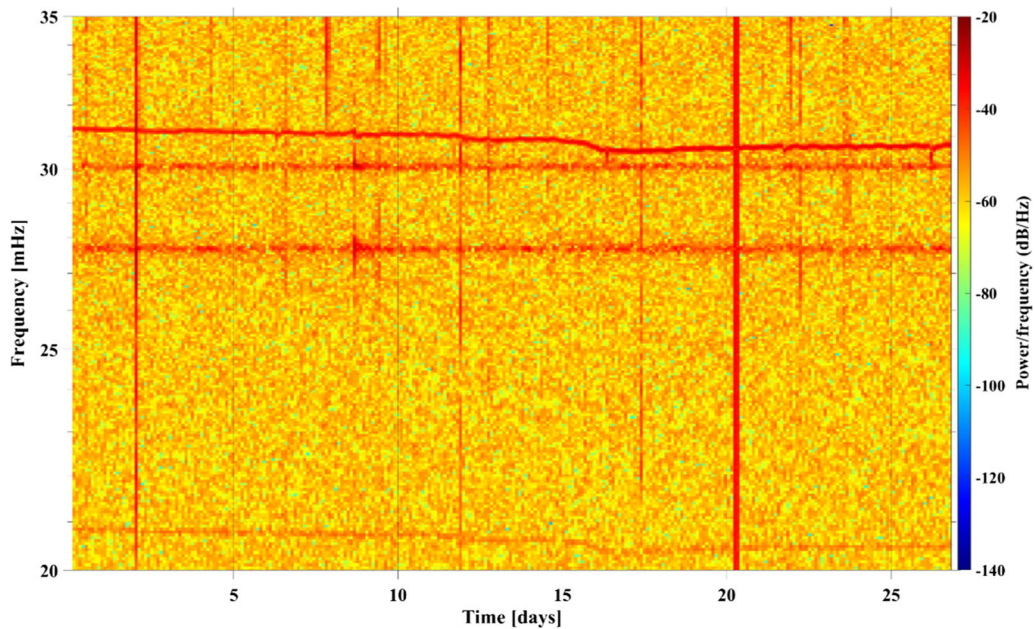


Figure 8  
Zoom in for Fig. 7 into range of characteristic frequencies

troubleshooting concerned the entire SG electronics, but ran parallel to a further steady deterioration of the data quality. In the end, the cause could be identified and repaired in SG electronics: It was a defective internal power supply, one capacitor was changed in the power supply unit (this will be further discussed in the section with the reanimation). However, the troubleshooting was not successful until the end of March 2013, so that a gap of several months could not be prevented. After the repair, the original data quality was immediately restored.

The long-term registration of the SG in Moxa was continued until 2020, so that further scientific results could be successfully achieved, in particular on the overlapping hydro-effect and oceanic loads. In 2020, problems arose again, which initially led to individual spikes and later to a significant increase in the overall noise level (Fig. 9). This time, the so-called SG auxiliary data, i.e. the control data on the neck temperatures and the two tilt components, were also affected. It was not apparent whether, for example, the disturbances in the tilt sensors were the cause of the noise in the gravimetric data or whether the tilt measurements were affected by the disturbances only

in the same way as the two superconducting sensor spheres.

In order to understand this malfunction of the SG, let us now analyze the data from July 2019, almost one year before the issues appeared. Figure 10 shows (according to Fig. 6) the according residuals and some intervals with low standard deviation. There are few new features which do not compare to the spectra in Fig. 6. First of all, the white noise floor of the instrument ( $> 200\text{mHz}$ ) as well as the amplitude in the frequency range  $100\text{mHz} < f < 200\text{mHz}$  is strongly increased. The characteristic frequency are not small width peaks. They form a significant feature with about ten times higher amplitudes. On top the standard deviation values are a factor 3 – 5 higher than in July 2002.

This is also clearly observable in the JTFA in Figs. 11 and 12. There are only the characteristic frequencies for the individual spheres visible. However, the whole frequency range of those frequencies is elevated in amplitude, ref. to Fig. 12. Thus, the other two signals, which are of lower amplitude (ref. Figure 8) are not observable.

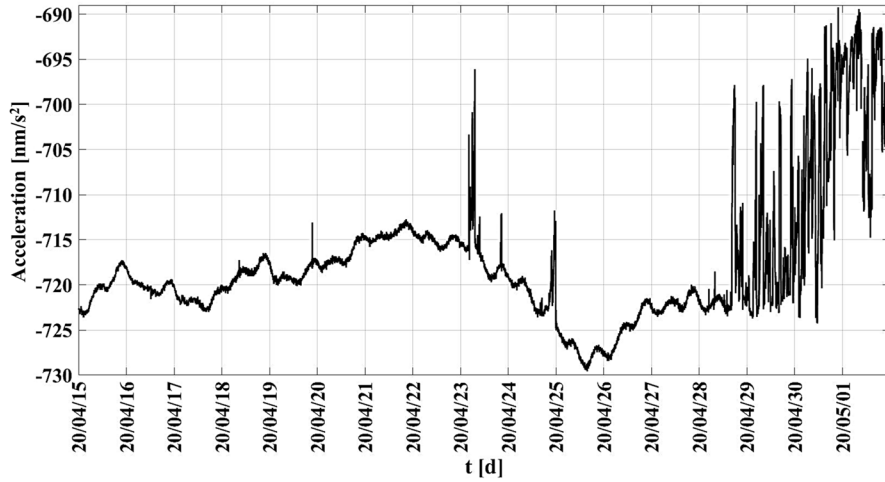


Figure 9  
SG residuals for the lower sensor from April 15, 2020 to May 01, 2020. Lower sensor data in  $\text{nm/s}^2$

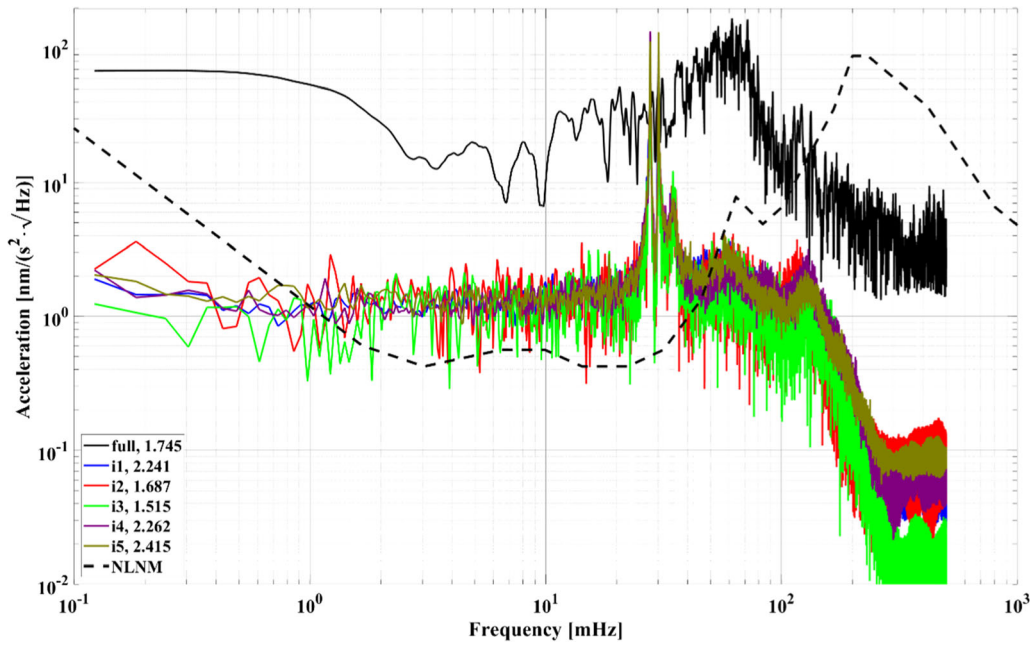


Figure 10  
Difference signal  $\Delta r$  of the SG CD-034 for July 2019. The full time series and intervals of it are marked by full and  $i_k$  in the legend. The numbers correspond to the according standard deviation in  $\text{nm}_{\text{RMS}}/\text{s}^2$  (RMS – root mean square)



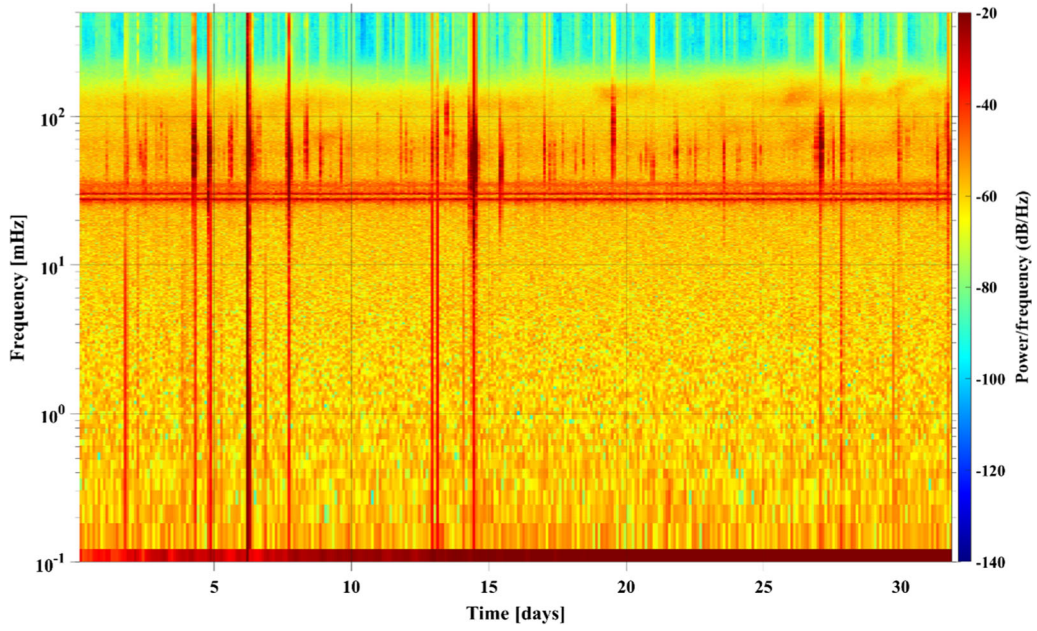


Figure 11  
Residual of the SG recording at Moxa Observatory for July 2019

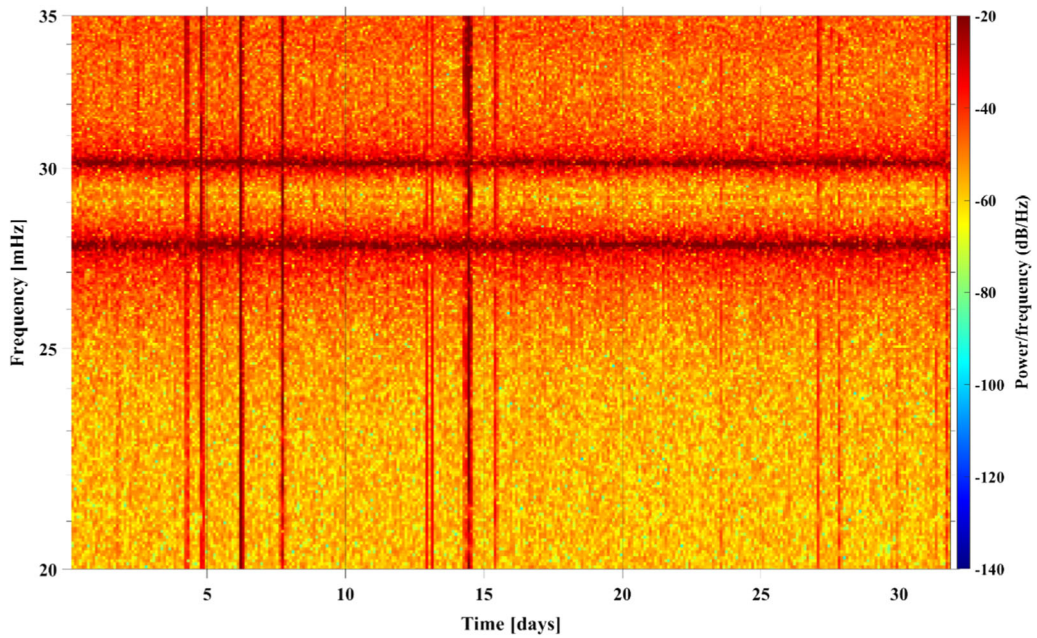


Figure 12  
Zoom in for Fig. 11 into range of characteristic frequencies

This gives a clear indication that the degradation of the SG's performance happened gradually and it is already observable by these methods one year ago. As a consequence, it is advisable for the instrument's operators to control the signals more carefully by making use of the methods introduced and discussed herein.

#### 4.3. Reanimation of the SG in July 2021

Before March 2021 the performance of the CD-034 degraded by then in a clearly observable manner like in 2013 again. This was obvious by an increase of the white band noise figure of the two channels. Finally, the noise increased more than a factor of hundred for frequencies  $> 200\text{mHz}$  of the Fourier spectrum, c.f. Figure 13 in comparison to Fig. 3, and one tilt sensor failed operation. The inspection revealed that the power supply voltage of  $\pm 15\text{V}$  had drop-outs and had ripples of more than 70%. There were also spikes with amplitudes exceeding  $\pm 100\text{mV}$  on the  $+15\text{V}$  power supply voltage observable. The main cause was identified: degradation and

failure of the used electrolytic capacitors in the instrument electronics. The primary mechanism for this is a slow evaporation of the electrolyte over time. Higher ambient and device internal temperatures speed up this process. Finally, it results in lower capacitance and higher effective series resistance. All electrolytic capacitors on all electronic boards of the power supply, instrument control, readout of gravimeter, tilt and temperatures were exchanged. These measures led for the SG CD-034 to a stable power supply with ripples of less than  $\pm 5\text{mV}$ . However, there are still sporadic spikes on the  $+15\text{V}$  power supply voltage now with lower amplitudes of  $\pm 100\text{mV}$  observable. The instrument is ever since fully operational again and the noise levels are at the expected or former values or even a bit lower than these.

The authors want to provide service to the community of users of SGs of this series by advising to:

- 1) Install an extra connector at the front or rear panel of the SG control rack with the power supply

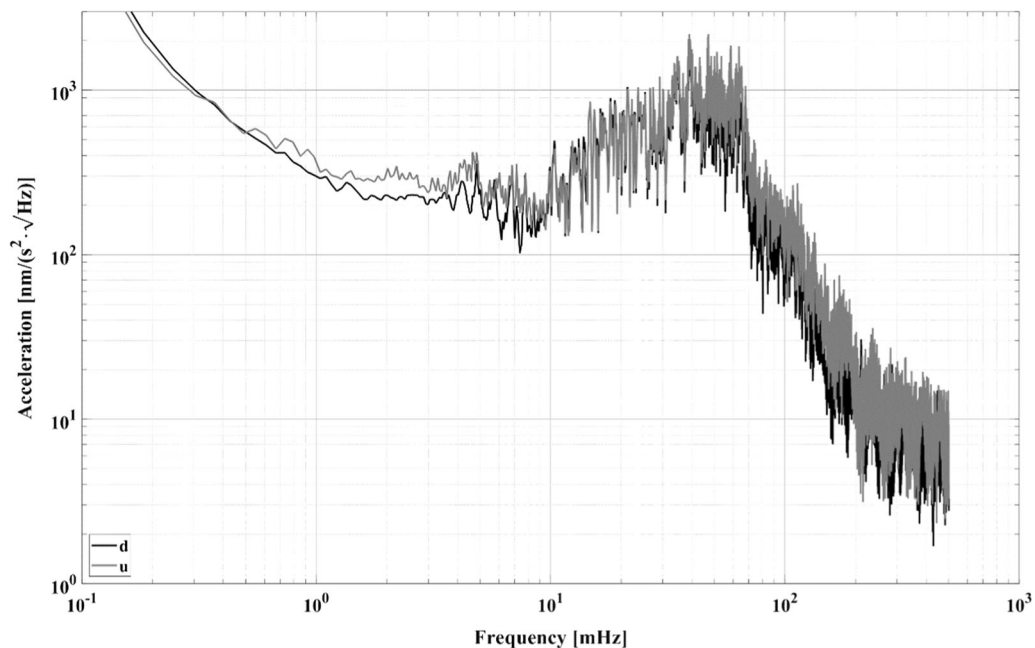


Figure 13  
Noise spectra for the signals of the two spheres in March 2021



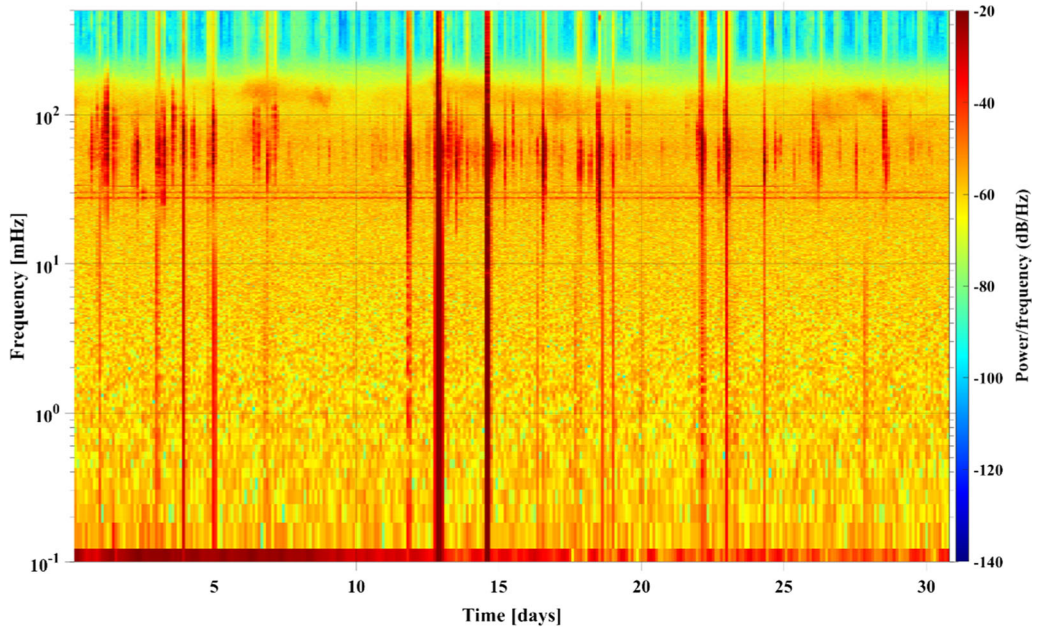


Figure 14  
Residual of the SG recording at Moxa Observatory for August 2021

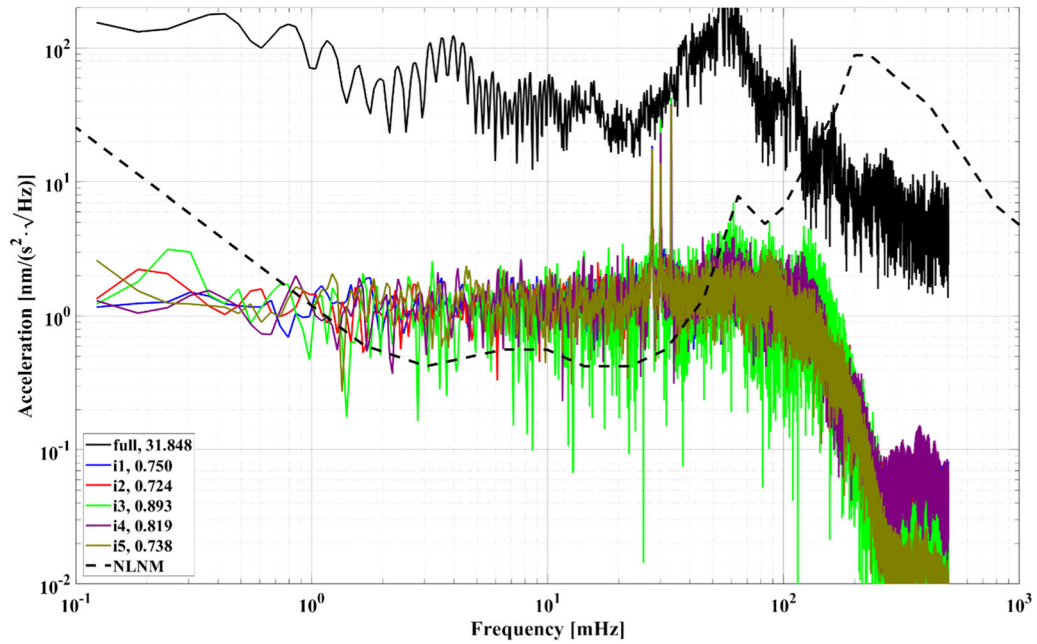


Figure 15  
Difference signal  $\Delta r$  of the SG CD-034 for August 2021. The full time series and intervals of it are marked by full and  $ik$  in the legend

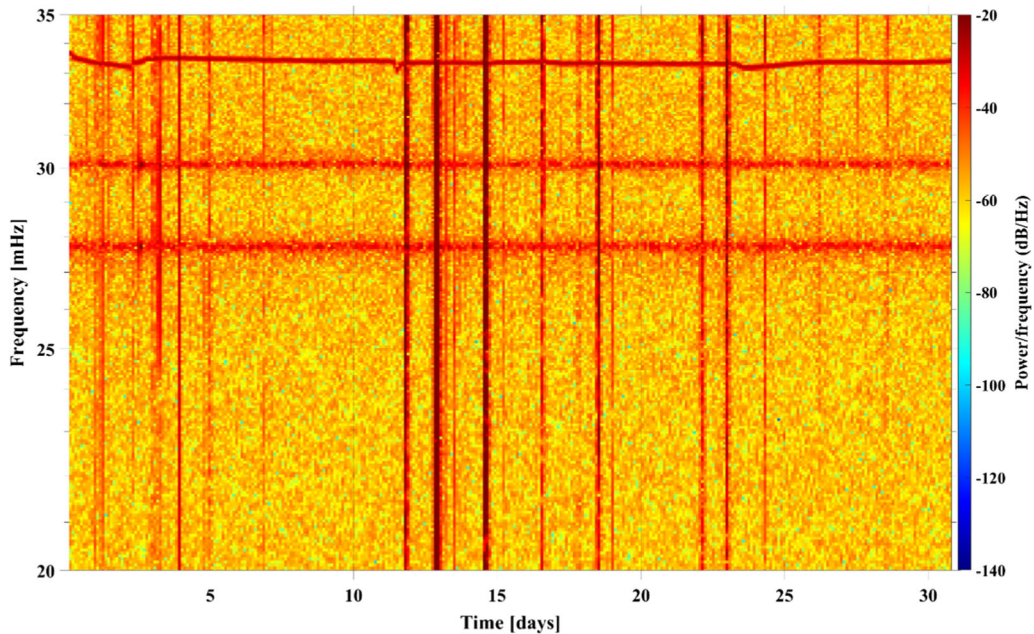


Figure 16  
Zoom in for Fig. 14 into range of characteristic frequencies

voltages in order to be able to control them by using an oscilloscope,

- 2) Exchange the electrolytic capacitors in a regular interval,
- 3) Be aware that the wiring colors inside of these units may NOT match the expected values of red (positive supply voltage), blue (negative supply voltage), and black (ground potential).

#### 4.4. Data Quality After Repair of the SG in August 2021

In August 2021 the SG CD-034 turned into continuous and low-noise operation again. A detailed inspection of the recorded data of August 2021 with the methods introduced herein revealed that the data quality turned into the expected level, refer to Fig. 14 until Fig. 15. The standard deviations went to values which are slightly higher than the levels measured in 2002. The sphere's characteristic frequencies in Fig. 16 turn out to be unchanged and one of the changing frequencies is now observable again. The whole range around the characteristic frequencies

returned to the expected level. Thus, one can conclude that the repair was successful.

However, there are still differences in the noise level for frequencies  $> 200\text{mHz}$ . For a number of years the SG CD-034 shows higher noise level compared to Fig. 7. It is not clear whether this is a gradual or abrupt change in the years from 2000 up to today. Further investigations are required on the whole long-term time series to get handle on the cause of this observation.

#### 4.5. Analytical Importance of the Described Methods

In this section another example will be shown which proves the importance of these methods for analyzing the data of the SG CD-034 at Observatory Moxa. During the course of these investigations, time series for July of some other years were processed. Interestingly, in June 2015 an abrupt change of the time series was identified. It is also clearly visible in the difference signal, c.f. Figure 17, with the same indications as for July 2019. This abrupt change is nicely observable in Figs. 18 and 19. The SG is going

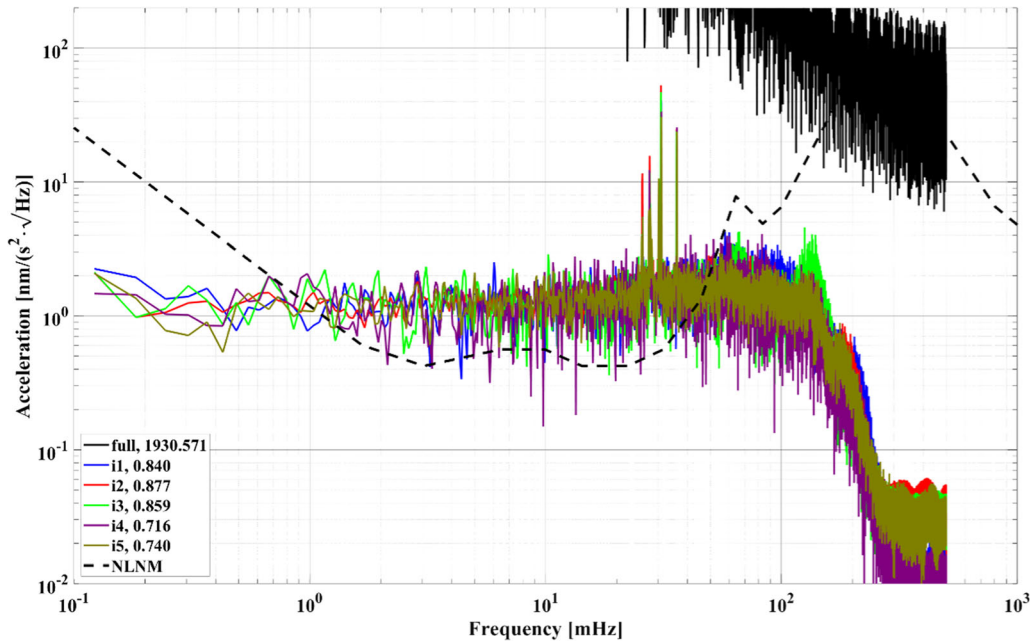


Figure 17

Difference signal  $\Delta r$  of the SG CD-034 for June 2015. The full time series and intervals of it are marked by full and *ik* in the legend

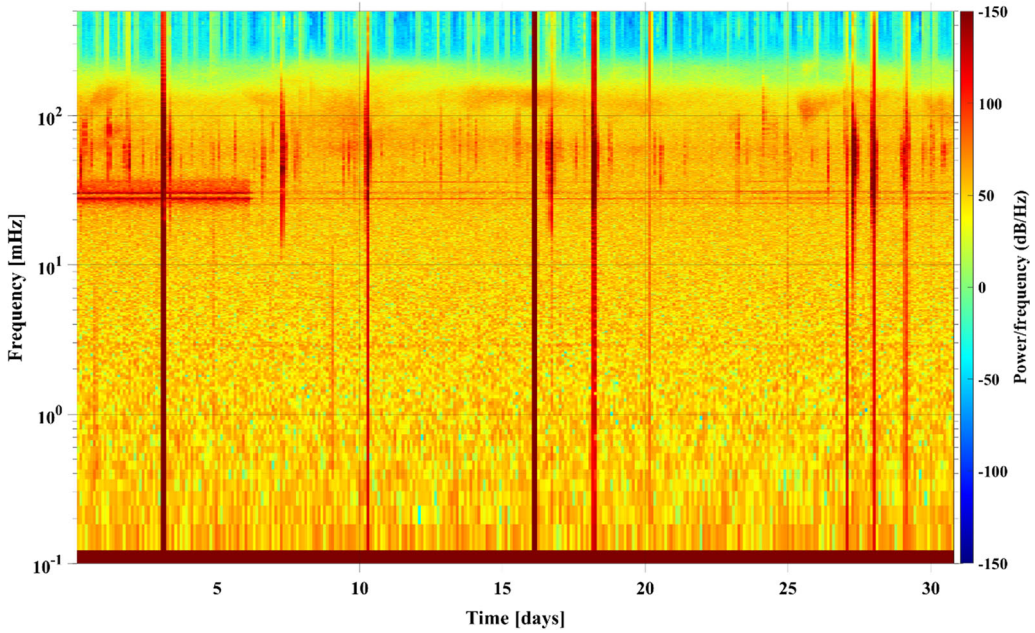


Figure 18

Residual of the SG recording at the Observatory Moxa for July 2015



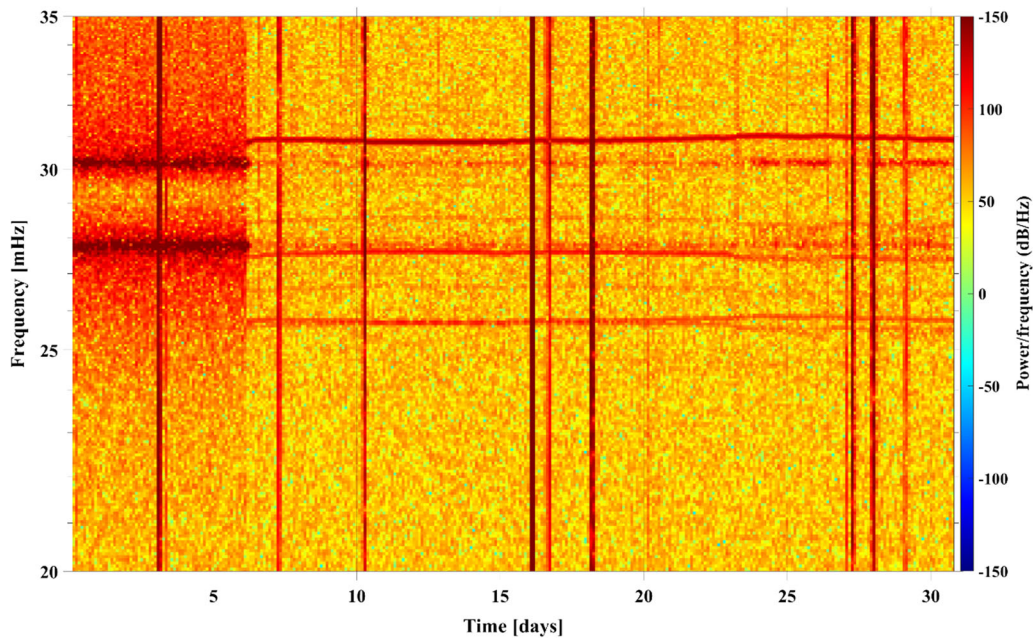


Figure 19  
Zoom in for Fig. 18 into range of characteristic frequencies

Table 1

*Tidal analysis of 110 days beginning at October 15, 2021 from SG CD-034 at Moxa observatory, after repair of SG electronics and restart of the recording in July 22, 2021*

| Theoretical description                            |   |      |   |            |                |   |                                   |
|--|---|------|---|------------|----------------|---|-----------------------------------|
| From [cpd]   | To [cpd]  | Wave | Ampl. [ $\text{nm}/\text{s}^2$ ]                                      | Ampl. fac. | Ampl. fac. std | Ph. lead [deg]                              | Std [ $\text{deg}_{\text{RMS}}$ ] |
| 0.600001   | 0.910000  | Q1   | 58.3534   | 1.14568    | 0.00078        | -0.2906                                     | 0.0376                            |
| 0.910001   | 0.949000  | O1   | 304.7724  | 1.14911    | 0.00018        | 0.0907                                      | 0.0088                            |
| 0.949001   | 0.980000  | M1   | 23.9574   | 1.15317    | 0.00213        | 0.2318                                      | 0.1061                            |
| 0.980001   | 1.012000  | K1   | 428.4649  | 1.13605    | 0.00011        | 0.1675                                      | 0.0055                            |
| 1.012001   | 1.050000  | J1   | 23.9657   | 1.15266    | 0.00215        | 0.0263                                      | 0.1069                            |
| 1.050001   | 1.500000  | OO1  | 13.1058   | 1.15838    | 0.00364        | -0.0584                                     | 0.1801                            |
| 1.500001   | 1.875000  | 2N2  | 9.2453  | 1.15952    | 0.00172        | 2.7097                                      | 0.0850                            |
| 1.875001   | 1.910000  | N2   | 57.8875   | 1.17808    | 0.00043        | 2.2793                                      | 0.0210                            |
| 1.910001   | 1.950000  | M2   | 302.3377  | 1.18581    | 0.00009        | 1.4825                                      | 0.0043                            |
| 1.950001   | 1.985000  | L2   | 8.5465  | 1.17242    | 0.00145        | 0.6927                                      | 0.0708                            |
| 1.985001   | 2.500000  | S2   | 140.6510  | 1.18293    | 0.00021        | 0.2135                                      | 0.0101                            |
| 2.500001   | 3.500000  | M3   | 3.7707  | 1.06946    | 0.00409        | 0.2105                                      | 0.2189                            |
| 3.500001   | 7.000000  | M4M6 | 0.0437  | 0.09964    | 0.27826        | -94.4568                                    | 160.0093                          |
| Adjusted meteorological or hydrological parameters |   |      |   |            |                |   |                                   |
| No. of data blocks                                 | Regr. coeff. [ $\text{nm}/(\text{s}^2 \times \text{hPa})$ ] |      | Std regr. [ $\text{nm}_{\text{RMS}}/(\text{s}^2 \times \text{hPa})$ ] |            |                | Std [ $\text{nm}_{\text{RMS}}/\text{s}^2$ ] |                                   |
| 1  | -3.46080  |      | 0.01423   |            |                | 0.530                                       |                                   |

Table 2

Comparison of tidal analyses: 110 days in 2015 before and in 2021 after repair of SG electronics. The data intervals were chosen for same standard deviations resulted by the tidal analyses

| Analysis: 2015 |  |                                 |  |                           | Analysis: 2021                               |                                  |  |                           |
|----------------|--|---------------------------------|--|---------------------------|--|----------------------------------|--|---------------------------|
| Total          | Std: 0.530 nm <sub>RMS</sub> /s <sup>2</sup> |                                 | Regr. coeff.: -3.39084 nm/(s <sup>2</sup> × hPa) |                           | Std: 0.530 nm <sub>RMS</sub> /s <sup>2</sup> |                                  | Regr. coeff.: -3.46080 nm/(s <sup>2</sup> × hPa) |                           |
| Wave           | Ampl [δ-factor]                              | Ampl. std [× 10 <sup>-6</sup> ] | Ph. lead [deg]                                   | Std [deg <sub>RMS</sub> ] | Ampl [δ-factor]                              | Ampl. std. [× 10 <sup>-6</sup> ] | Ph. lead [deg]                                   | Std [deg <sub>RMS</sub> ] |
| O1             | 1.14921                                      | 190                             | 0.0897   | 0.0093                    | 1.14911                                      | 180                              | 0.0907   | 0.0088                    |
| K1             | 1.13594                                      | 170                             | 0.1873   | 0.0084                    | 1.13605                                      | 110                              | 0.1675   | 0.0055                    |
| M2             | 1.18546                                      | 80                              | 1.4804   | 0.0039                    | 1.18581                                      | 90                               | 1.4825   | 0.0043                    |
| N2             | 1.17907                                      | 360                             | 1.9914   | 0.0177                    | 1.17808                                      | 430                              | 2.2793   | 0.0210                    |

from a disturbed state into the normal, low-noise state on the 6th of July 2015.

It is remarkable, since standard processing did not show any issue in the operation. Additionally, there is no recording from the operators that any changes have been done in this period. The transition is also remarkable since, for instance, after the rapid change the expected specific frequency of 30.0mHz for the lower sensor signal seems only to appear again at the 23rd of July 2015. A new review on the time series data and further investigations are required to understand whether this happens frequently and what the cause of these disturbances of the SG operation is.

### 5. Tidal Analyses and Discussion

An essential question arising from the repair of SG electronics is whether or not the important calibration factors for the two sensing spheres have changed due to the renewal of numerous electronic modules in the control and data acquisition of the SG. For a data interval of 110 days from 15 October 2021, a tidal analysis was calculated, but due to the short time interval, this was only for 13 tidal waves. The comparison with data from the same period for 2015 is intended to indicate whether or not modified calibration factors must be assumed. For the tidal analysis, ETERNA3.4 (Wenzel, 1996) with the tidal potential of Hartmann and Wenzel (1995) was used. The results are listed in Table 1. For the tidal waves with the largest amplitudes O1, K1, M2 and N2 the

tidal amplitude factors become stable with small errors. This is also shown for the analyzed phases. These analysis results were compared with an analysis result from 2015, calculated also for a time span of 110 days in this year, refer to Table 2. The criteria for choosing the same data quality for both timeseries intervals was the standard deviation, provided by the tidal analyses.

The comparison with a corresponding analysis of 2015 data, which shows the largest diurnal and semi-diurnal tidal waves (Table 2), proves that calculated tidal parameters coincide very well with the respective amplitude. It also confirms that the SG's repair obviously has not changed the calibration factors of the individual sensors. The ratios of M2/O1 for 2015 (= 1.03154) and for 2021 (= 1.03194) deviate by  $5 \cdot 10^{-4}$  which is smaller than the accuracy of the calibration factor. Thus, the consistency of calibration before and after the repair is confirmed by these analyses. Of course, this comparison will be repeated for longer time series and the absolute gravity measurements realized by the team at BKG will be continued in order to verify the validity of the calibration for both sensors.

### 6. Conclusions

Superconducting Gravimeters are in continuous use world wide and operated by many different countries. In particular, the very long-term recording of geosignals such as the pole movement can be



detected globally and continuously in this way. For high-quality analyses and interpretations, gravimeters must be installed for years or even decades to provide the required long period, uninterrupted time series data. In addition to the actual gravimetric sensors, this naturally also applies to the controlling electronics, as well as to other adapted components, such as, for example, the cold head, the inclination compensation and various internal control sensors.

Continuous long-term operation necessarily leads to an aging of the entire system, including the installed electronics. The components contained therein, such as for example, the capacitors or internal power supplies may degrade or even fail operation. For this process the control of the signals and noise levels by Fourier spectra, standard deviation, and even JTFA are introduced in this paper which is of utmost importance. The new processing steps reveal details of the degradation of the SG's performance. Examples of the malfunctioning of the SG in Moxa are shown and discussed. Even a so far unknown event has been identified with the new methods.

The slow but continuous aging process has also increasingly disturbed and finally even ended the long-term registration without gaps in the Observatory Moxa. Only an extensive renewal of all affected electronic modules made it possible to continue operation of the SG CD-034, but at this time a gap of several months had already been unavoidable. This was the case after more than 20 years of permanent registration; the repair took place in July 2021. For long-term observations with SGs, we recommend, as a result of our experience, after a period of about 10 to 15 years of continuous operation, to check the entire detection and control electronics with regard to the damage caused by the aging and, if necessary, to renew affected components. If successful, long gaps without data recording could be avoided.

#### *Acknowledgements*

The repair work described here was carried out by the Leibniz IPHT employee Frank Bauer. The adequate handling of the SG in the Observatory Moxa was guaranteed by the participation of Wernfrid Kühnel.

Thank you very much for your great and extensive commitment. We would like to thank our technical staff Matthias Meininger and Marcus Möller for their support and especially Adelheid Weise for her intensive discussion and support by the recalculation of the SG residuals. Previous members of the Moxa team who are largely responsible for the results described in the text should also be mentioned with gratitude: Gerhard Jentzsch, Corinna Kroner, Adelheid Weise, Kasper Fischer, Chris Salomon, André Gebauer and Holger Steffen. The absolute measurement team of the BKG, Andreas Reinhold, Reinhard Falk and now André Gebauer are thanked for their repeated measurements in Moxa. The General Geophysics Group of the Institute of Geosciences and the staff of Leibniz IPHT in Jena were thanked for their support for our work at the Moxa Geodynamic Observatory. The English language was improved by Glenn Chubak which is gratefully acknowledged. The authors would like to thank two anonymous reviewers for the very constructive and valuable comments and notes in the text and for the figures.

#### *Funding*

Open Access funding enabled and organized by Projekt DEAL. 1, 1, Thomas Jahr, 2, 2, Ronny Stolz. Open Access This article is licensed under a Creative Commons Attribution 4.0 International License, which permits use, sharing, adaptation, distribution and reproduction in any medium or format, as long as you give appropriate credit to the original author(s) and the source, provide a link to the Creative Commons licence, and indicate if changes were made. The images or other third party material in this article are included in the article's Creative Commons licence, unless indicated otherwise in a credit line to the material. If material is not included in the article's Creative Commons licence and your intended use is not permitted by statutory regulation or exceeds the permitted use, you will need to obtain permission directly from the copyright holder. To view a copy of this licence, visit <http://creativecommons.org/licenses/by/4.0/>.

### Data Availability Statement

All SG gravity data sets used in this study are freely available from the data bank provided by IGETS (Boy et al., 2020) or by contacting the Geodynamic Observatory Moxa/Germany.

**Publisher's Note** Springer Nature remains neutral with regard to jurisdictional claims in published maps and institutional affiliations.

### REFERENCES

- Boy, J.-P., Barriot, J.-P., Förste, C., Voigt, C. & Wziontek, H., (2020). Achievements of the first 4 years of the International Geodynamics and Earth Tide Service (IGETS) 2015–2019. IAG Symp. [https://doi.org/10.1007/1345\\_2020\\_94](https://doi.org/10.1007/1345_2020_94).
- Hartmann, T., & Wenzel, H.-G. (1995). Catalogue HW95 of the tide generating potential. *Bull. Inf. Marées Terrestres*, 123, 9278–9301.
- Hinderer, J., Crossley, D., & Warburton, R. J. (2007). Gravimetric methods – superconducting gravity meters. In G. Schubert (Ed.), *Treatise on geophysics* (Vol. 3, pp. 65–122). Elsevier. ISBN 9780444527486.
- Hinderer, J., Crossley, D., & Warburton, R. (2015). *Superconducting Gravimetry*. Elsevier.
- Jahr, T., & Weise, A. (2020). Storm surges in the German bight: are they detectable as gravity field variations at the geodynamic observatory Moxa in Thuringia, Germany? *Allgemeine Vermessungsnachrichten (AVN)*, 4(127), 182–190.
- Jahr, T., Jentzsch, G., & Kroner, C. (2001). The geodynamic observatory Moxa/Germany; instrumentation and purposes. *Journal of the Geodetic Society of Japan*, 47(1), 34–39.
- Klinge K. (2000). Moderne Breitband- und Array-Seismologie in Deutschland: In: 100 Jahre seismologische Forschung in Jena. *Mitt. der Deutschen Geophysikalischen Gesellschaft IV/2000*.
- Klügel, T., & Wziontek, H. (2009). Correcting gravimeters and tiltmeters for atmospheric mass attraction using operational weather models. *Journal of Geodynamics*, 48(3–5), 204–210.
- Krause, P., Naujoks, M., Fink, M., & Kroner, C. (2009). The impact of soil moisture changes on gravity residuals obtained with a superconducting gravimeter. *Journal of Hydrology*, 373(1–2), 151–163.
- Kroner, C., & Jahr, T. (2006). Hydrological experiments around the superconducting gravimeter at Moxa observatory. *Journal of Geodynamics*, 41(1–3), 268–275.
- Kroner, C., & Weise, A. (2011). Sensitivity of superconducting gravimeters in central Europe on variations in regional river and drainage basins. *Journal of Geodesy*, 85(10), 651–659.
- Kroner, C., Jahr, T., Naujoks, M., & Weise, A. (2007). Hydrological signals in gravity — foe or friend? In P. Tregoning & C. Rizos (Eds.), *Dynamic planet: monitoring and understanding a dynamic planet with geodetic and oceanographic tools* (pp. 504–510). Springer. ISBN 978-3-540-49350-1.
- Kroner C. (2002). Zeitliche Variationen des Erdschwerefeldes und ihre Beobachtungen mit einem supraleitenden Gravimeter im Geodynamischen Observatorium Moxa: Habilitation thesis. *Jenaer Geowissenschaftliche Schriften* 2.
- Naujoks, M., Weise, A., Kroner, C., & Jahr, T. (2008). Detection of small hydrological variations in gravity by repeated observations with relative gravimeters. *Journal of Geodesy*, 82(9), 543–553.
- Niebauer, T. (2015). Gravimetric methods absolute and relative gravity meter: instruments concepts and implementation. *Treatise on Geophysics* (pp. 37–57). Elsevier. ISBN 9780444538031.
- Oppenheim, A. V., & Schaffer, R. W. (2014). *Discrete-time signal processing*. Pearson New international edition.
- Peterson, J. R. (1993). Observations and modeling of seismic background noise. *Open-File Report, U.S. Geological Survey*. <https://doi.org/10.3133/of93322>
- Richter B., & Warburton, R.J. (1998). A New Generation of Superconducting Gravimeters. In: *Proc. 13th Symp. Earth Tides*, 13th Symp. Earth Tides, Brussels, Belgium, pp. 545–555.
- Rosat, S. (2002). A comparison of the seismic noise levels at various GGP stations. *Bull. Inf. Marées Terrestres*, 135, 10689–10700.
- Rosat, S., & Hinderer, J. (2011). Noise levels of superconducting gravimeters: updated comparison and time stability. *Bulletin of the Seismological Society of America*, 101(3), 1233–1241.
- Stoer, J., & Bulirsch, R. (2002). *Introduction to numerical analysis* (Vol. 12). Springer. ISBN 9780387954523.
- Stoica, P., & Moses, R. L. (2005). *Spectral analysis of signals*. Pearson Prentice Hall. ISBN 0131139568.
- Teupser, C. (1975). The seismological station of Moxa, in seismology and solid-earth-physics. *Veröffentlichungen Des Zentralinstituts Physik Der Erde*, 14, 577–584.
- van Camp, M., de Viron, O., Watlet, A., Meurers, B., Francis, O., & Caudron, C. (2017). Geophysics from terrestrial time-variable gravity measurements. *Reviews of Geophysics*, 55(4), 938–992.
- Weise, A., & Jahr, T. (2018). The improved hydrological gravity model for Moxa observatory, Germany. *Pure and Applied Geophysics PAGEOPH*, 175(5), 1755–1763.
- Weise, A., Kroner, C., Abe, M., Ihde, J., Jentzsch, G., Naujoks, M., Wilmes, H., & Wziontek, H. (2009). Gravity field variations from superconducting gravimeters for GRACE validation. *J. Geodyn.*, 48(3–5), 325–330.
- Weise, A., Kroner, C., Abe, M., Creutzfeldt, B., Förste, C., Güntner, A., Ihde, J., Jahr, T., Jentzsch, G., Wilmes, H., Wziontek, H., & Petrovic, S. (2012). Tackling mass redistribution phenomena by time-dependent GRACE- and terrestrial gravity observations. *Journal of Geodynamics*, 59–60(18), 82–91.
- Wenzel, H.-G. (1996). The nanogal software: Earth tide data processing package ETERNA 3.30. *Bull. Inf. Marées Terrestres*, 124, 9425–9439.